

High Accuracy Evaluation of the Finite Fourier Transform using Sampled Data

Eugene A. Morelli
*NASA Langley Research Center
Hampton, Virginia*

June 1997

National Aeronautics and Space Administration
Langley Research Center
Hampton, Virginia 23681-0001

Table of Contents

Abstract.....	iii
Nomenclature	iv
I. Introduction.....	1
II. Theoretical Development.....	2
III. Examples.....	9
IV. Summary.....	11
V. Acknowledgments	11
VI. References	12
Appendix – Derivation of the Cubic Interpolation Formulae.....	13
Figures.....	19

Abstract

Many system identification and signal processing procedures can be done advantageously in the frequency domain. A required preliminary step for this approach is the transformation of sampled time domain data into the frequency domain. The analytical tool used for this transformation is the finite Fourier transform. Inaccuracy in the transformation can degrade system identification and signal processing results. This work presents a method for evaluating the finite Fourier transform using cubic interpolation of sampled time domain data for high accuracy, and the chirp z -transform for arbitrary frequency resolution. The accuracy of the technique is demonstrated in example cases where the transformation can be evaluated analytically. Arbitrary frequency resolution is shown to be important for capturing details of the data in the frequency domain. The technique is demonstrated using flight test data from a longitudinal maneuver of the F-18 High Alpha Research Vehicle.

Nomenclature

f	cyclic frequency, Hz
FFT	Fast Fourier Transform
i	time index
j	imaginary number = $\sqrt{-1}$
k	frequency index
M	number of discrete frequencies
N	number of sampling intervals
t	time, sec
T	data record length, sec
P_n	n th order Lagrange interpolating polynomial
$x(t)$	real function of time t
x_i	sampled $x(t)$ at time $i\Delta t$
\tilde{x}_k	discrete Fourier transform of x_i for frequency f_k
$\tilde{x}(f)$	finite Fourier transform of $x(t)$ for frequency f
W	interior point cubic weighting function
α	angle of attack, deg
Δt	sampling interval, sec
φ	endpoint interpolation function
γ	endpoint cubic weighting function
θ	discrete Fourier transform angular step
ω	frequency, rad / sec
ψ	interior point interpolation function

superscripts

\sim	Fourier transform
$*$	complex conjugate

I. Introduction

Data analysis and linear parametric modeling can be carried out in either the time domain or the frequency domain¹. Frequency domain analysis has many advantages, including physical insight, direct applicability to control system design, and lower dimensionality for model parameter estimation, among others¹⁻³. Frequency domain techniques based on spectral estimation³⁻⁵, output error¹⁻³, and equation error^{1,6,7} have been used successfully for flight test data analysis and modeling. The basis for all of these frequency domain methods is the finite Fourier transform, which is the mechanism for transforming time domain data to the frequency domain. Any errors in the transformation from time to frequency domain affect the accuracy of the raw data in the frequency domain, which in turn impacts data analysis and modeling results.

Typically, transformation from the time domain to frequency domain is brought about using sampled time domain data and a simple Euler approximation of the finite Fourier integral. This calculation, called the discrete Fourier transform, can be implemented with a Fast Fourier Transform (FFT) algorithm⁸ for increased computational speed. The simple Euler approximation makes the discrete Fourier transform increasingly inaccurate with increasing frequency and sampling time. Accuracy of transformation to the frequency domain can be improved using various quadrature methods⁸, which involve evaluating the Fourier integral separately for each individual frequency of interest.

For a given data record length, the discrete Fourier transform constrains the frequency resolution to equal the reciprocal of the record length. As the record length decreases, frequency resolution can become coarse, leading to omission of important data features in the frequency domain. One solution to this problem is to pad the time domain data with zeros and thus artificially increase the data record length, but this is inconvenient and increases processing time. It is also possible to interpolate values in the frequency domain, but this is also inconvenient and can be inaccurate as well. When the frequency band of interest is relatively small, most of the processing involved in the discrete Fourier transform is for frequencies outside the range of interest, since the computations include all frequencies up to the Nyquist frequency.

The purpose of this work is to present a convenient and efficient method for computing the finite Fourier transform with high accuracy using sampled data, while allowing a wide range of choice for the frequency band and frequency resolution. This capability gives a solid underpinning to the many frequency domain techniques developed and renders those methods commensurately more accurate and flexible.

The next section outlines the theory for the flexible, high accuracy finite Fourier transform method. Following that, some realistic simulation examples are presented to demonstrate some of the issues discussed in the theory. Finally, an example using measured flight test data from the F-18 High Alpha Research Vehicle is included.

II. Theoretical Development

The Fourier transform of a continuous scalar time function $x(t)$ on a finite time interval $[0, T]$ is called the *finite Fourier transform*, and is defined by

$$\tilde{x}(f) \equiv \int_0^T x(t) e^{-j2\pi ft} dt \quad (1)$$

or

$$\tilde{x}(\omega) \equiv \int_0^T x(t) e^{-j\omega t} dt \quad (2)$$

where

$$\omega = 2\pi f \quad (3)$$

When the time function $x(t)$ is sampled at discrete evenly spaced time intervals, the finite Fourier transform can be approximated by

$$\tilde{x}(f) \approx \Delta t \sum_{i=0}^{N-1} x_i e^{-j2\pi ft_i} \quad (4)$$

where

$$t_i \equiv i\Delta t \quad , \quad x_i \equiv x(t_i) = x(i\Delta t) \quad i = 0, 1, 2, \dots, N \quad (5)$$

and

$$\Delta t = \frac{T}{N} \quad (6)$$

Eq. (4) is a simple Euler approximation for the integral in Eq. (1), using the first N discrete values of the continuous time function $x(t)$. Note from Eq. (5) that the total number of samples is $N + 1$. The discrete Fourier transform can be used to evaluate the summation in Eq. (4) at specific frequencies. The discrete Fourier transform is defined by

$$\tilde{x}_k \equiv \sum_{i=0}^{N-1} x_i e^{-j2\pi f_k t_i} \quad k = 0, 1, 2, \dots, M-1 \quad (7)$$

where

$$f_k = \frac{k}{N\Delta t} = \frac{k}{T} \quad k = 0, 1, 2, \dots, M-1 \quad (8)$$

and

$$M = \begin{cases} N/2 & \text{for } N \text{ even} \\ (N+1)/2 & \text{for } N \text{ odd} \end{cases} \quad (9)$$

The values given for M in Eq. (9) represent the fundamental limitation that frequencies contained in a sampled time history must fall within the frequency band $[0, f_n)$ (i.e., below f_n), where f_n is the Nyquist frequency, defined as one half the sampling frequency:

$$f_n \equiv \frac{1}{2\Delta t} \quad (10)$$

For the discrete frequencies f_k in Eq. (8), using Eq. (7) in Eq. (4) gives

$$\tilde{x}(f_k) \approx \Delta t \tilde{x}_k \quad k = 0, 1, 2, \dots, M-1 \quad (11)$$

The discrete Fourier transform in Eq. (7) can be expressed in another form by substituting from Eqs. (5) and (8) to obtain

$$\tilde{x}_k = \sum_{i=0}^{N-1} x_i e^{-j2\pi ik/N} \quad k = 0, 1, 2, \dots, M-1 \quad (12)$$

Now define

$$\theta \equiv \omega_k \Delta t = 2\pi f_k \Delta t = \frac{2\pi k}{N} \quad k = 0, 1, 2, \dots, M-1 \quad (13)$$

where the dependence of θ on k is not shown explicitly by the notation. Using Eq. (13), Eq. (12) can be written as

$$\tilde{x}_k = \sum_{i=0}^{N-1} x_i e^{-j\theta i} \quad k = 0, 1, 2, \dots, M-1 \quad (14)$$

Combining Eqs. (12)-(14), and (4),

$$\tilde{x}(\theta) = \tilde{x}(2\pi f_k \Delta t) \approx \Delta t \tilde{x}_k \quad k = 0, 1, 2, \dots, M-1 \quad (15)$$

When N is an integer power of 2, FFT algorithms⁸ can be used to efficiently carry out the summation in Eq. (12).

Eqs. (7) and (8) indicate that the discrete Fourier transform is defined for frequencies which correspond to an integral number of cycles for each time period T . Since the finite Fourier transform is an integration over the time interval $[0, T]$, the values computed using the approximation in Eq. (15) can be small, and thus susceptible to round-off error accumulated during the summation in Eq. (12). In addition, since Eq. (15) represents a simple Euler approximation to the integral in Eq. (1), high frequencies f_k or large sample times Δt will introduce additional inaccuracy because of the oscillatory nature of the integrand. The latter difficulty was recognized as early as 1928 by Filon⁹, who proposed an interpolation scheme for the sampled time domain data to improve the accuracy of finite Fourier integrals. The same basic approach is taken here, using a cubic Lagrange polynomial interpolation due to Press et al.⁸. The resulting calculation uses the discrete Fourier transform with weighting factors as follows:

$$\begin{aligned} \tilde{x}(\theta) \approx \Delta t \{ & W(\theta) [\tilde{x}_k + x_N e^{-j\theta N}] \\ & + \gamma_0(\theta)x_0 + \gamma_1(\theta)x_1 + \gamma_2(\theta)x_2 + \gamma_3(\theta)x_3 \\ & + e^{j\theta T/\Delta t} [\gamma_0^*(\theta)x_N + \gamma_1^*(\theta)x_{N-1} + \gamma_2^*(\theta)x_{N-2} + \gamma_3^*(\theta)x_{N-3}] \} \end{aligned} \quad (16)$$

where

$$W(\theta) = \left(\frac{6 + \theta^2}{3\theta^4} \right) (3 - 4\cos\theta + \cos 2\theta) \approx 1 - \frac{11}{720}\theta^4 + \frac{23}{15120}\theta^6 \quad (17)$$

and

$$\begin{aligned}\gamma_0(\theta) &= \frac{(-42 + 5\theta^2) + (6 + \theta^2)(8\cos\theta - \cos 2\theta)}{6\theta^4} - j \frac{(-12\theta + 6\theta^3) + (6 + \theta^2)\sin 2\theta}{6\theta^4} \\ &\approx -\frac{2}{3} + \frac{1}{45}\theta^2 + \frac{103}{15120}\theta^4 - \frac{169}{226800}\theta^6 - j\theta\left(\frac{2}{45} + \frac{2}{105}\theta^2 - \frac{8}{2835}\theta^4 + \frac{86}{467775}\theta^6\right)\end{aligned}\quad (18)$$

$$\begin{aligned}\gamma_1(\theta) &= \frac{14(3 - \theta^2) - 7(6 + \theta^2)\cos\theta}{6\theta^4} - j \frac{30\theta - 5(6 + \theta^2)\sin\theta}{6\theta^4} \\ &\approx \frac{7}{24} - \frac{7}{180}\theta^2 + \frac{5}{3456}\theta^4 - \frac{7}{259200}\theta^6 - j\theta\left(\frac{7}{72} - \frac{1}{168}\theta^2 + \frac{11}{72576}\theta^4 - \frac{13}{5987520}\theta^6\right)\end{aligned}\quad (19)$$

$$\begin{aligned}\gamma_2(\theta) &= \frac{-4(3 - \theta^2) + 2(6 + \theta^2)\cos\theta}{3\theta^4} - j \frac{-12\theta + 2(6 + \theta^2)\sin\theta}{3\theta^4} \\ &\approx -\frac{1}{6} + \frac{1}{45}\theta^2 - \frac{5}{6048}\theta^4 + \frac{1}{64800}\theta^6 - j\theta\left(-\frac{7}{90} + \frac{1}{210}\theta^2 - \frac{11}{90720}\theta^4 + \frac{13}{7484400}\theta^6\right)\end{aligned}\quad (20)$$

$$\begin{aligned}\gamma_3(\theta) &= \frac{2(3 - \theta^2) - (6 + \theta^2)\cos\theta}{6\theta^4} - j \frac{6\theta - (6 + \theta^2)\sin\theta}{6\theta^4} \\ &\approx \frac{1}{24} - \frac{1}{180}\theta^2 + \frac{5}{24192}\theta^4 - \frac{1}{259200}\theta^6 - j\theta\left(\frac{7}{360} - \frac{1}{840}\theta^2 + \frac{11}{362880}\theta^4 - \frac{13}{29937600}\theta^6\right)\end{aligned}\quad (21)$$

Detailed derivation of the expressions in Eqs. (16)-(21) can be found in the Appendix. The series expansions for $W(\theta)$, $\gamma_0(\theta)$, $\gamma_1(\theta)$, $\gamma_2(\theta)$, and $\gamma_3(\theta)$ given above are used for small θ , where θ is considered small when its magnitude is less than the largest value of θ for which identical results are obtained to machine precision with both the analytic expression and the series expansion. The series expansions are necessary because of high order cancellations that make the analytic expressions inaccurate when θ is small.

For many practical problems, such as flight test data analysis, only a relatively small frequency band is of interest. It is advantageous to select the frequencies in the finite Fourier transform to be closely spaced within the frequency band of interest to ensure that details of the frequency spectrum are accurately captured. Arbitrary frequency resolution in a selected frequency band can be achieved with the chirp z -transform¹⁰. The flexibility of the chirp z -transform allows high

resolution calculation of the Fourier integral in important regions of the frequency domain, with up to N discrete frequencies evenly spaced in a selected frequency band.

Suppose that M discrete frequencies are selected in the frequency band $[f_0, f_1)$,

$$f_k = f_0 + k \Delta f \quad k = 0, 1, 2, \dots, M-1 \quad (22)$$

where

$$\Delta f = \frac{(f_1 - f_0)}{M} \quad (23)$$

Then Eq. (7) can be written as

$$\tilde{x}_k = \sum_{i=0}^{N-1} x_i e^{-j2\pi f_k t_i} = \sum_{i=0}^{N-1} x_i e^{-j2\pi f_0 i \Delta t} e^{-j2\pi k \Delta f i \Delta t} \quad k = 0, 1, 2, \dots, M-1 \quad (24)$$

Defining

$$\phi_0 \equiv 2\pi f_0 \Delta t \quad , \quad \Delta\phi \equiv 2\pi \Delta f \Delta t \quad (25)$$

$$A \equiv e^{j\phi_0} \quad , \quad Z \equiv e^{j\Delta\phi} \quad (26)$$

and combining Eqs. (24)-(26),

$$\tilde{x}_k = \sum_{i=0}^{N-1} x_i A^{-i} Z^{-ki} = \sum_{i=0}^{N-1} x_i [AZ^k]^{-i} \quad (27)$$

As k increases, the quantity AZ^k represents a contour along the unit circle in the z plane. The quantity ϕ_0 is the angular location on the unit circle associated with the starting frequency f_0 , and $\Delta\phi$ represents the incremental angular step along the unit circle in the z plane for each frequency increment Δf , corresponding to each increment in k . Figure 1 illustrates the idea. Comparing Eqs. (14) and (24), and using Eq. (25),

$$\theta = \phi_0 + k\Delta\phi = 2\pi\Delta t(f_0 + k\Delta f) \quad k = 0, 1, 2, \dots, M-1 \quad (28)$$

Suppose the initial frequency is chosen as zero,

$$f_0 = 0 \quad , \quad \phi_0 = 0 \quad , \quad A = 1 \quad (29)$$

and the frequency increment is chosen as

$$\Delta f = \frac{1}{T} = \frac{1}{N\Delta t} \quad , \quad \Delta\phi = \frac{2\pi}{N} \quad , \quad Z = e^{j2\pi/N} \quad (30)$$

Then if the number of discrete frequencies M is chosen from Eq. (9), the chirp z -transform is identical to the discrete Fourier transform of Eq. (12). Using Eqs. (29) and (30) in Eq. (28),

$$\theta = k\Delta\phi = \frac{2\pi k}{N} \quad k = 0, 1, 2, \dots, M-1 \quad (31)$$

The choices in Eqs. (29) and (30) correspond to the case where the contour in the z plane consists of equal angular increments around the entire unit circle, which is identical to that for the discrete Fourier transform of Eq. (12), cf. Eqs. (13) and (31). Eqs. (7)-(9) indicate that the contour in the z plane for the discrete Fourier transform completes nearly a half circle from $\theta = 0$ up to but not including $\theta = \pi$, which corresponds to the Nyquist frequency. For the chirp z -transform, the starting frequency and frequency increment are not restricted to the values given in Eqs. (29)-(30), but can be chosen arbitrarily. This translates to small angular increments over an arc of the unit circle in the z plane. The chirp z -transform is also called the zoom Fourier transform, because of the capability to achieve very fine resolution in the frequency domain for a selected frequency range.

A disadvantage of using the frequencies associated with the discrete Fourier transform (specified in Eqs. (8) and (9)) is that the spacing of these discrete frequencies depends on the data record length T . For short data records, the frequency resolution can be coarse, leading to a loss of fine detail in the frequency domain, with consequent degraded data analysis and modeling results. In extreme cases, it is possible for the discrete frequencies to be spaced such that significant features in the frequency domain are missed. In addition, the frequency points used in the discrete Fourier transform are evenly spaced between zero frequency and the Nyquist frequency f_n . For a small bandwidth of interest, this means that much of the computation is for frequencies outside the range of interest. The resulting number of usable data points in the

frequency domain can therefore be small, again to the detriment of the data analysis and modeling results.

The chirp z -transform decouples the frequency resolution from the length of the time record and can place all calculated frequency points within the frequency band of interest. The cubic interpolation corrections given above in Eqs. (16)-(21) apply without modification to the chirp z -transform because the chirp z -transform is just a discrete Fourier transform using discrete frequencies that can be adjusted arbitrarily, independent of the time record length. The penalty for this flexibility is more computation time, but the magnitude of this extra computation time continues to shrink as computing machinery becomes faster. It is possible to compute the chirp z -transform efficiently for arbitrary N using FFT algorithms¹⁰.

In summary, the procedure for computing the high accuracy chirp z cubic approximation to the finite Fourier transform is:

1. Choose the initial frequency f_0 and the number of frequency domain points M .
2. Choose the frequency resolution Δf , or choose the upper limit of the frequency band f_1 and compute Δf from Eq. (23).
3. Compute the values of θ from Eq. (28).
4. Use the chirp z -transform to carry out the summation in Eq. (14), which is equivalent to Eq. (27).
5. Compute the weighting factor and endpoint corrections from Eqs. (17)-(21) for each θ .
6. Use Eq. (16) to compute the high accuracy chirp z cubic approximation to the finite Fourier transform for each θ .

III. Examples

Figure 2 is a plot of an example time function, $x(t) = 1 - e^{-2t}$, $\Delta t = 0.05$, $T = 5$, which might represent the step response of a dynamical system. Figure 3 shows the magnitude and phase of the finite Fourier transform of $x(t)$ calculated using the Euler approximation of Eq. (15) and the cubic interpolation approximation of Eq. (16), compared to values calculated analytically using Eq. (1) for the same frequencies f_k from Eq. (8). The analytic values and the cubic approximation are very nearly identical, so that the associated traces are indistinguishable in Figure 3. The Euler approximation shows some inaccuracy in magnitude, with phase angle inaccuracy that increases with frequency. Figure 4 shows the differences in magnitude and phase between the analytic values and the approximate values, and Figure 5 is a plot of the percent errors based on the analytic values. All results in this work were computed using double precision arithmetic. Accuracy of the Euler approximation would be worse using single precision arithmetic because of the susceptibility of the calculation to round-off error, discussed previously. Figures 4 and 5 quantify the errors associated with using the Euler approximation and clearly show that the cubic interpolation scheme of Eq. (16) completely corrects the errors. This example demonstrates the high accuracy associated with the cubic interpolation scheme compared to the conventional Euler approximation.

Figure 6 is a different example time function, $x(t) = 5e^{-t} \sin(\pi t)$, $\Delta t = 0.05$, $T = 5$, which might represent the impulse response of a dynamical system. The frequency spectrum for this time function is mainly associated with the frequency of the sine function, in contrast to the last example where the frequency content was dominated by low frequencies near zero. In Figure 7, the Euler approximation of Eq. (15) is compared with the cubic interpolation approximation of Eq. (16) using the chirp z -transform to achieve frequency resolution ten times finer than that computed from Eq. (8) and used in the Euler approximation. The magnitude plot in Figure 7 shows that the Euler approximation does not capture the full detail of the frequency spectrum due to the relatively coarse resolution in the frequency domain resulting from Eq. (8). The horizontal scale covers only 0 to 2 Hz and does not extend to the full Nyquist frequency (10 Hz), in order to illustrate the frequency resolution. Figure 8 shows the differences in magnitude and phase between the analytic values and the approximations. The comparison of the Euler approximation with analytic values used the frequencies from Eq. (8), while the comparison of the chirp z cubic approximation to analytic values used the tenfold higher frequency resolution. Figure 8 is therefore an accuracy check analogous to Figure 4, and shows that the chirp z cubic approximation is also accurate for the higher frequency resolution. At higher frequencies not shown in Figure 8, the phase angle error for the Euler approximation increases in a fashion similar to that seen in Figure 4 for the last example. This example demonstrates that the chirp z cubic approximation can not only provide details of the frequency spectrum that are missed with the coarse frequency resolution of the Euler approximation, but also produces values that are highly accurate for the finer frequency resolution of the chirp z cubic approximation.

Figure 9 shows angle of attack measurements taken during a 15 second longitudinal flight test maneuver flown on the F-18 High Alpha Research Vehicle. The sampling rate was 50 Hz. Figure 10 shows the corresponding magnitude and phase angle results computed using the Euler approximation of Eq. (15) and the chirp z cubic approximation of Eq. (16) with a frequency resolution ten times finer than that computed from Eq. (8) and used in the Euler approximation. The frequency scale covers 0 to 1.4 Hz, because all the rigid body dynamics lie in this frequency band. In general, it is not necessary to choose the frequency resolution to be an integer multiple of the f_k from Eq. (8) for the chirp z cubic approximation. In fact, Eqs. (22) and (23) indicate that the frequency resolution is arbitrary, with the only limitation being that the frequency steps associated with Z in Eq. (26) will be the same for each increment in k . It is also possible to move the frequency band of interest anywhere below the Nyquist frequency by choosing f_0 and f_1 . This might be desired to investigate high frequency structural modes, for example. For the chirp z cubic approximation, it was therefore possible to place all the computed frequency domain points in the frequency band given above, with no wasted calculations. In contrast, the Euler approximation computes values for frequencies f_k out to the Nyquist frequency (25 Hz), but the only values of interest are associated with f_k in the frequency band 0 to 1.4 Hz. As in the previous example, the chirp z cubic approximation captures details of the frequency spectrum that were missed using the coarse frequency resolution of Eq. (8). In signal processing and system identification applications, this corresponds to an increase in the number of data points in the frequency domain, which generally improves results. In Figure 11, the differences between magnitude and phase computed using the Euler approximation and the chirp z cubic approximation are plotted for the frequencies used in the Euler approximation (f_k from Eq. (8)). Figure 12 shows the magnitude and phase differences between the two approximations for all f_k from Eq. (8) out to the Nyquist frequency. Although it is not possible to assess the accuracy of the approximations for flight test data because the analytic values are unknown, it can be seen that the phase differences in Figure 12 show an increase with frequency that is similar to what was seen in the simulation example cases.

IV. Summary

A high accuracy method for computing the finite Fourier transform for sampled time domain data was presented and demonstrated with examples. The technique uses cubic interpolation of the sampled time data in the integrand of the finite Fourier transform, and employs the chirp z -transform to achieve arbitrary resolution in the frequency domain regardless of the length of the time record. Accuracy improvement was demonstrated using examples, and the effect of full control over frequency resolution independent of the length of the time record was demonstrated. Although other quadrature methods can be used to accurately compute the finite Fourier transform, the technique presented here has the advantages of convenient and efficient calculation, while at the same time achieving high accuracy and arbitrary frequency resolution.

V. Acknowledgments

Discussions with Dr. Vladislav Klein of the George Washington University and Dr. Pat Murphy of NASA Langley and their critical reviews of this work are acknowledged and appreciated.

VI. References

1. Klein, V. "Aircraft Parameter Estimation in Frequency Domain", AIAA paper 78-1344, Atmospheric Flight Mechanics Conference, Palo Alto, CA, August 1978.
2. Klein, V., "Maximum Likelihood Method for Estimating Airplane Stability and Control Parameters from Flight Data in Frequency Domain", NASA TP 1637, May 1980.
3. Tischler, M.B., "Frequency-Response Identification of the XV-15 Tilt-Rotor Aircraft Dynamics", NASA TM 89428, May 1987.
4. Otnes, R.K. and Enochson, L. *Applied Time Series Analysis, Volume 1, Basic Techniques*, John Wiley & Sons, New York, NY, 1978.
5. Bendat, J.S. and Piersol, A.G. *Random Data Analysis and Measurement Procedures*, 2nd Ed., John Wiley & Sons, New York, NY, 1986.
6. Pearson, A.E., Shen, Y., and Klein, V., "Application of Fourier Modulating Functions to Parameter Estimation of a Multivariable Linear Differential System", 10th IFAC Symposium on System Identification, Preprints Vol. 3, Copenhagen, Denmark, July 1994, pp. 49-54.
7. Pearson, A.E., "Aerodynamic Parameter Estimation Via Fourier Modulating Function Techniques", NASA CR 4654, April 1995.
8. Press, W.H., et al., *Numerical Recipes (FORTRAN version)*, 2nd Ed., Cambridge University Press, New York, NY, 1989.
9. Filon, L.N.G., "On a Quadrature Formula for Trigonometric Integrals", *Proceedings of the Royal Society of Edinburgh*, Vol. 49, 1928, pp. 38-47.
10. Rabiner, L.R., Schafer, R.W., and Rader, C.M., "The Chirp z -Transform Algorithm and Its Application", *The Bell System Technical Journal*, May-June 1969, pp. 1249-1292.

Appendix – Derivation of the Cubic Interpolation Formulae

To accurately evaluate the finite Fourier transform in Eq. (1), Lagrange polynomials are used to interpolate samples of the function $x(t)$ in the integrand. This avoids the inaccuracy associated with the Euler approximation of the integral represented by the calculations in Eqs. (14) and (15). Lagrange interpolating polynomials have the property that they pass through each data point. The n th order Lagrange interpolating polynomial is given by⁸

$$P_n(t) = \sum_{m=0}^n \frac{\ell_m(t)}{\ell_m(t_m)} x_m \quad (\text{A-1})$$

where

$$\ell_m(t) = \prod_{\substack{j=0 \\ j \neq m}}^n (t - t_j) = \frac{(t - t_0)(t - t_1)(t - t_2) \dots (t - t_n)}{(t - t_m)} \quad (\text{A-2})$$

For n th order interpolation, $n + 1$ function values are required and the n th order Lagrange interpolating polynomial includes $n + 1$ n th order functions of t weighted by neighboring discrete function values. Cubic interpolation therefore requires four function values, two on either side of the interval for which the interpolation is being done. The functions $\ell_m(t)$ are simple n th order polynomials in t . In Figure A-1, the sampled function value x_i at a typical interior point t_i is shown to be involved in the interpolation when t falls within any of four different intervals, namely, (t_{i-2}, t_{i-1}) , (t_{i-1}, t_i) , (t_i, t_{i+1}) , and (t_{i+1}, t_{i+2}) . The endpoints would be involved in fewer intervals. The first and last interval have to use three points on one side (toward the interior of the data record) and the endpoint. Outside of these intervals for t , the i th function value does not contribute to the interpolation. A general interpolation expression for the function $x(t)$ can then be written as

$$x(t) \approx \sum_{i=0}^N x_i \psi(t) + \sum_{i=\text{endpoints}} x_i \varphi_i(t) \quad (\text{A-3})$$

where the $\varphi_i(t)$ multiplying the endpoint function values must account for the endpoints being included in the first summation as if they were regular interior points. Applying the finite Fourier transform to both sides of Eq. (A-3),

$$\tilde{x}(\omega) \approx \int_0^T \left\{ \sum_{i=0}^N x_i \psi(t) + \sum_{i=\text{endpoints}} x_i \varphi_i(t) \right\} e^{-j\omega t} dt \quad (\text{A-4})$$

Introducing the change of variable

$$s = (t - t_i) / \Delta t \quad (\text{A-5})$$

for integral of the first summation, so that $s_{i-1} = (t_{i-1} - t_i) / \Delta t = -1$, $s_i = (t_i - t_i) / \Delta t = 0$, $s_{i+1} = (t_{i+1} - t_i) / \Delta t = 1$, etc. This is equivalent to mapping t_i to zero on the s axis and normalizing the sampling interval to unity. For the integral of the second summation, introduce the change of variable

$$s = t / \Delta t \quad (\text{A-6})$$

which has similar effects. Making the substitutions and using Eq. (5), Eq. (A-4) then becomes

$$\tilde{x}(\omega) \approx \Delta t \int_{-\infty}^{\infty} \left\{ \sum_{i=0}^N x_i \psi(s) e^{-j\omega i \Delta t} e^{-j\omega \Delta t s} + \sum_{i=\text{endpoints}} x_i \varphi_i(s) e^{-j\omega \Delta t s} \right\} ds \quad (\text{A-7})$$

The limits of the integration in s can be set to $\pm\infty$ because both $\psi(s)$ and $\varphi(s)$ are zero outside a finite range of s values. Switching the order of integration and differentiation, and denoting $\theta = \omega \Delta t$ as in Eq. (13), Eq. (A-7) becomes

$$\tilde{x}(\omega) \approx \Delta t \left\{ W(\theta) \sum_{i=0}^N x_i e^{-j\theta i} + \sum_{i=\text{endpoints}} x_i \gamma_i(s) \right\} \quad (\text{A-8})$$

or

$$\tilde{x}(\omega) \approx \Delta t \left\{ W(\theta) \left[x_N e^{-j\theta N} + \sum_{i=0}^{N-1} x_i e^{-j\theta i} \right] + \sum_{i=\text{endpoints}} x_i \gamma_i(s) \right\} \quad (\text{A-9})$$

where

$$W(\theta) = \int_{-\infty}^{\infty} \psi(s) e^{-j\theta s} ds \quad (\text{A-10})$$

$$\gamma_i(\theta) = \int_{-\infty}^{\infty} \phi_i(s) e^{-j\theta s} ds \quad (\text{A-11})$$

The expressions in Eqs. (A-10) and (A-11) need only be evaluated once for a particular interpolation scheme. The first summation in Eq. (A-9) is recognized as the discrete Fourier transform from Eq. (14). For cubic interpolation, using Eq. (14) in Eq. (A-9) gives

$$\begin{aligned} \tilde{x}(\theta) \approx \Delta t \{ & W(\theta) [\tilde{x}_k + x_N e^{-j\theta N}] \\ & + \gamma_0(\theta) x_0 + \gamma_1(\theta) x_1 + \gamma_2(\theta) x_2 + \gamma_3(\theta) x_3 \\ & + e^{j\theta T/\Delta t} [\gamma_0^*(\theta) x_N + \gamma_1^*(\theta) x_{N-1} + \gamma_2^*(\theta) x_{N-2} + \gamma_3^*(\theta) x_{N-3}] \} \end{aligned} \quad (\text{A-12})$$

which is identical to Eq. (16).

From Eqs. (A-1), (A-2), and (A-5), the Lagrange polynomial in s multiplying an interior point x_i for the interpolation labeled 1 in Figure A-1 is

$$\psi_1(s) = \frac{(s+3)(s+2)(s+1)}{6} \quad (\text{A-13})$$

Similarly, for the interpolations labeled 2, 3, and 4 in Figure A-1, the Lagrange polynomials in s multiplying an interior point x_i are

$$\psi_2(s) = \frac{(s+2)(s+1)(s-1)}{-2} \quad (\text{A-14})$$

$$\psi_3(s) = \frac{(s+1)(s-1)(s-2)}{2} \quad (\text{A-15})$$

$$\psi_4(s) = \frac{(s-1)(s-2)(s-3)}{-6} \quad (\text{A-16})$$

Since an interior point x_i is involved in only the four interpolations shown in Figure A-1,

$$\psi(s) = \psi_1(s) + \psi_2(s) + \psi_3(s) + \psi_4(s) \quad (\text{A-17})$$

Using Eq. (A-17) in Eq. (A-10) with appropriate integration limits gives

$$W(\theta) = \int_{-2}^{-1} \psi_1(s) e^{-j\theta s} ds + \int_{-1}^0 \psi_2(s) e^{-j\theta s} ds + \int_0^1 \psi_3(s) e^{-j\theta s} ds + \int_1^2 \psi_4(s) e^{-j\theta s} ds \quad (\text{A-18})$$

Substituting the expressions in Eqs. (A-13)-(A-16) into Eq. (A-18) results in a straightforward integration problem. Evaluating the integrals and simplifying, the result is

$$W(\theta) = \left(\frac{6 + \theta^2}{3\theta^4} \right) (3 - 4 \cos \theta + \cos 2\theta) \quad (\text{A-19})$$

The corresponding Taylor series expansion about $\theta = 0$ is

$$W(\theta) = \left(\frac{6 + \theta^2}{3\theta^4} \right) (3 - 4 \cos \theta + \cos 2\theta) \approx 1 - \frac{11}{720} \theta^4 + \frac{23}{15120} \theta^6 \quad (\text{A-20})$$

which is identical to Eq. (17).

For the points near the end of the data record, Eq. (A-11) applies with the coordinate s running in the negative direction toward the interior of the data,

$$\gamma_{N-i}(\theta) = \int_{-\infty}^{-\infty} \varphi_{N-i}(-s) e^{-j\theta(N-s)} (-ds) = e^{-j\theta N} \int_{-\infty}^{\infty} \varphi_i(s) e^{j\theta s} ds = e^{-j\theta T/\Delta t} \gamma_i^*(\theta) \quad (\text{A-21})$$

where

$$\varphi_i(s) = \varphi_{N-i}(-s) \quad (\text{A-22})$$

since the interpolations at the start and end of the record are mirror images of one another. Eq. (A-21) shows that computing endpoint corrections for the beginning of the sampled data will also provide corrections for points at the end.

In Eq. (A-12), $W(\theta)$ is applied to the discrete points near the beginning and end of the record as if they were interior points. The endpoint correction terms make adjustments relative to this to give the appropriate calculation for the endpoints. For example, the fourth point of the data record (x_3) is involved in the same four interpolations that an interior point is involved in, but also is involved in the interpolation in the first interval, (t_0, t_1) , where three points must be used on the right side of the interval ($x_1, x_2,$ and x_3), along with the initial point x_0 . Figure A-2 illustrates the situation. The correction factor for the fourth point therefore represents the contribution of the fourth point to the interpolation for the first interval. The Lagrange polynomial multiplying the fourth point for interpolation in the first interval is

$$\varphi_3(s) = \frac{s(s-1)(s-2)}{6} \quad (\text{A-23})$$

Using the appropriate limits, the endpoint correction can be evaluated from

$$\gamma_3(\theta) = \int_0^1 \varphi_3(s) e^{-j\theta s} ds = \int_0^1 \left[\frac{s(s-1)(s-2)}{6} \right] e^{-j\theta s} ds \quad (\text{A-24})$$

Evaluating the integral and simplifying,

$$\gamma_3(\theta) = \frac{2(3 - \theta^2) - (6 + \theta^2) \cos \theta}{6\theta^4} - j \frac{6\theta - (6 + \theta^2) \sin \theta}{6\theta^4} \quad (\text{A-25})$$

The corresponding Taylor series expansion about $\theta = 0$ is

$$\begin{aligned}\gamma_3(\theta) &= \frac{2(3 - \theta^2) - (6 + \theta^2)\cos\theta}{6\theta^4} - j\frac{6\theta - (6 + \theta^2)\sin\theta}{6\theta^4} \\ &\approx \frac{1}{24} - \frac{1}{180}\theta^2 + \frac{5}{24192}\theta^4 - \frac{1}{259200}\theta^6 - j\theta\left(\frac{7}{360} - \frac{1}{840}\theta^2 + \frac{11}{362880}\theta^4 - \frac{13}{29937600}\theta^6\right)\end{aligned}\quad (\text{A-26})$$

which is identical to Eq. (21).

For $\gamma_0(\theta)$, $\gamma_1(\theta)$, and $\gamma_2(\theta)$, the contribution for the first interval interpolation is included in a fashion similar to that shown for $\gamma_3(\theta)$ above. In addition, for $\gamma_0(\theta)$, $\gamma_1(\theta)$, and $\gamma_2(\theta)$, one or more terms must be subtracted to account for the fact that x_0 , x_1 , and x_2 are not involved in all four interpolations shown in Figure A-1 for an interior point. For example, $\gamma_2(\theta)$ includes the contribution to the first interval interpolation for x_2 , along with a subtraction for one of the four interpolations shown in Figure A-1 which does not apply for x_2 . The contribution for this interpolation has been included in the $W(\theta)$ term of Eq. (A-12) for x_2 and must therefore be subtracted in the endpoint correction term. The expression for $\gamma_2(\theta)$ is then

$$\gamma_2(\theta) = \int_0^1 \left[\frac{s(s-1)(s-3)}{-2} \right] e^{-j\theta s} ds - \int_{-2}^{-1} \psi_1(s) e^{-j\theta s} ds \quad (\text{A-27})$$

where $\psi_1(s)$ is given by Eq. (A-13). Comparing Eqs. (A-27) and (A-11),

$$\begin{aligned}\varphi_2(s) &= \frac{s(s-1)(s-3)}{-2} & 0 \leq s \leq 1 \\ \varphi_2(s) &= \psi_1(s) = \frac{(s+3)(s+2)(s+1)}{6} & -2 \leq s \leq -1 \\ \varphi_2(s) &= 0 & \text{otherwise}\end{aligned}\quad (\text{A-28})$$

so that $\varphi_2(s)$ is seen to be a function that has non-zero values only for s in the intervals $(0, 1)$ or $(-2, -1)$. The other endpoint corrections $\gamma_0(\theta)$ and $\gamma_1(\theta)$ are computed similarly.

Figures

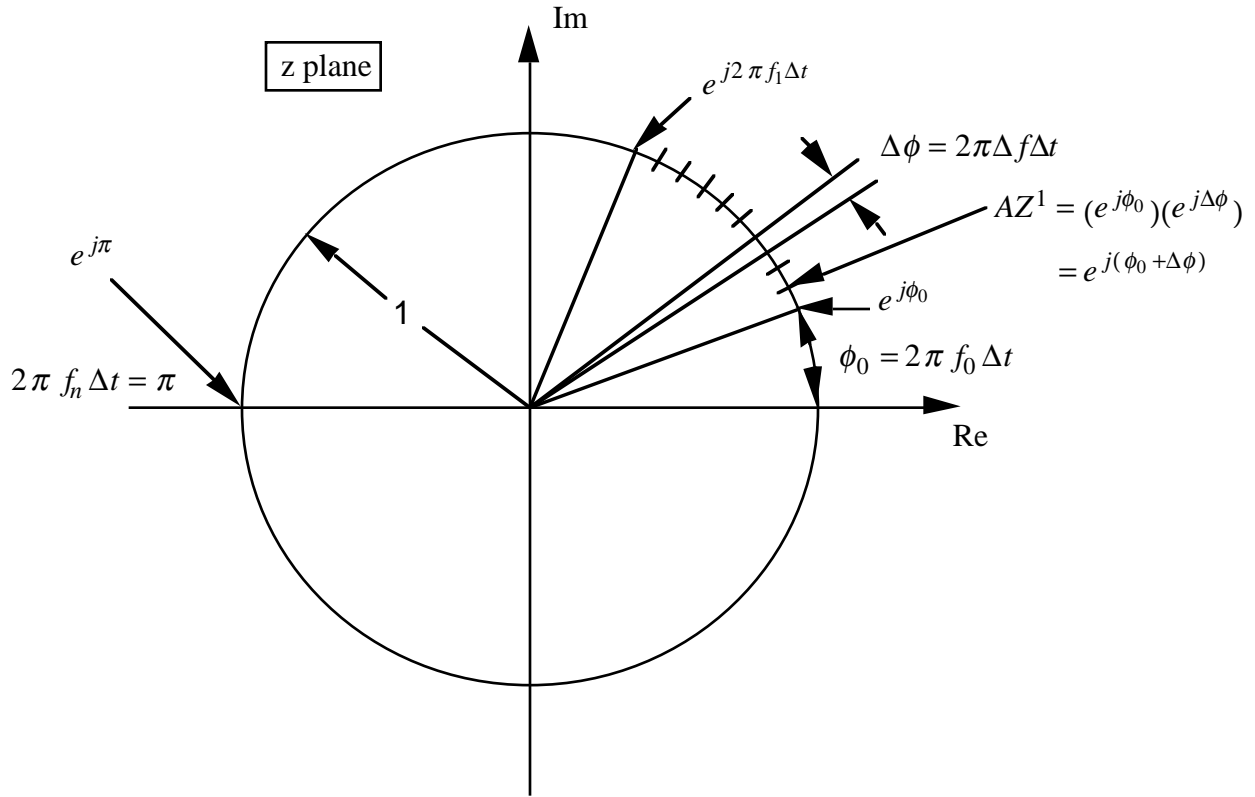


Figure 1 Chirp z-Transform Diagram

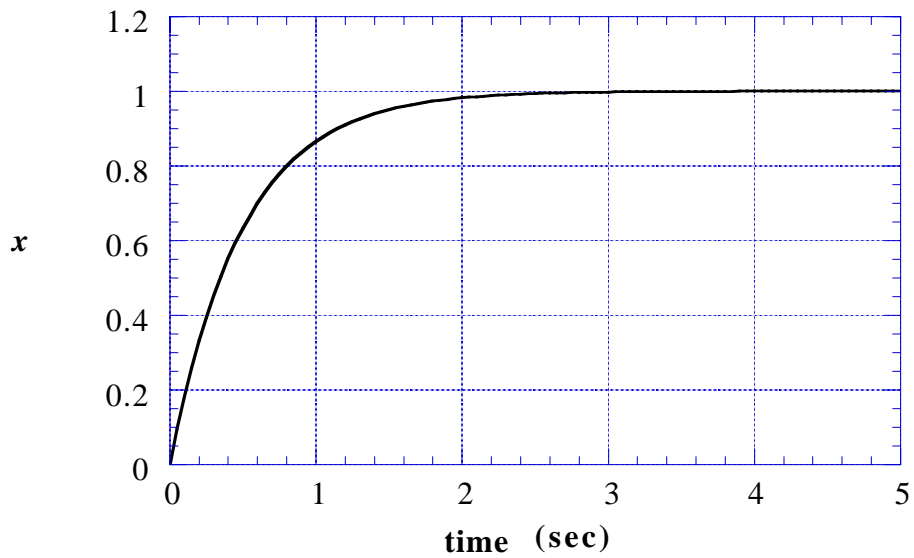


Figure 2 Example Time History

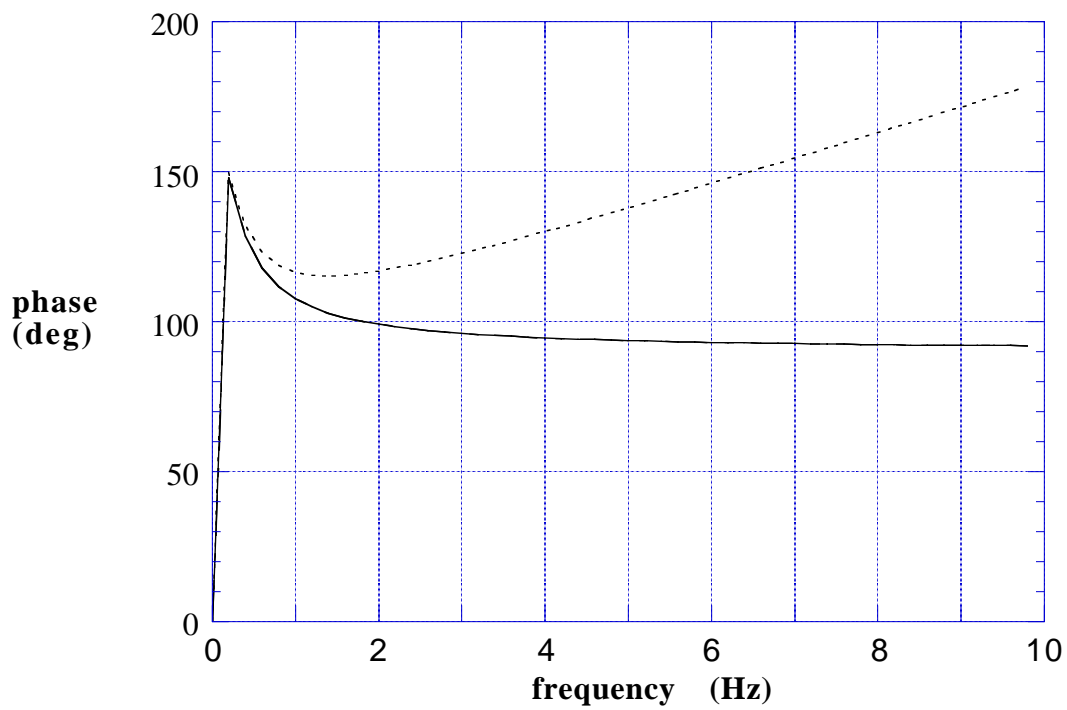
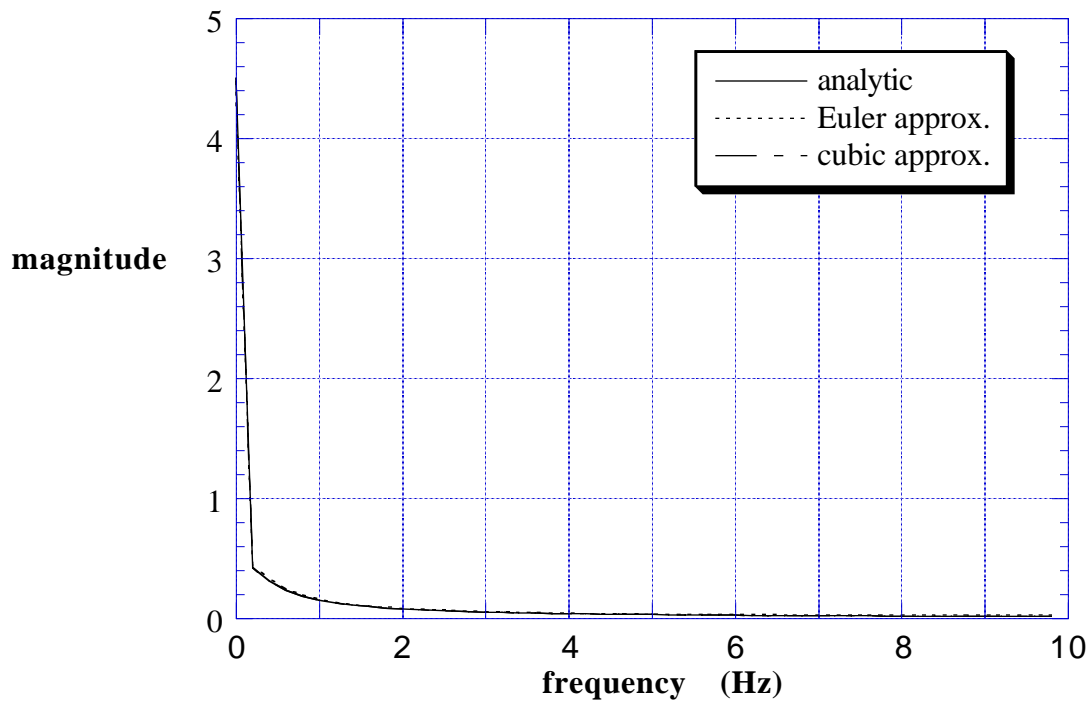


Figure 3 Finite Fourier Transform Calculation Comparison

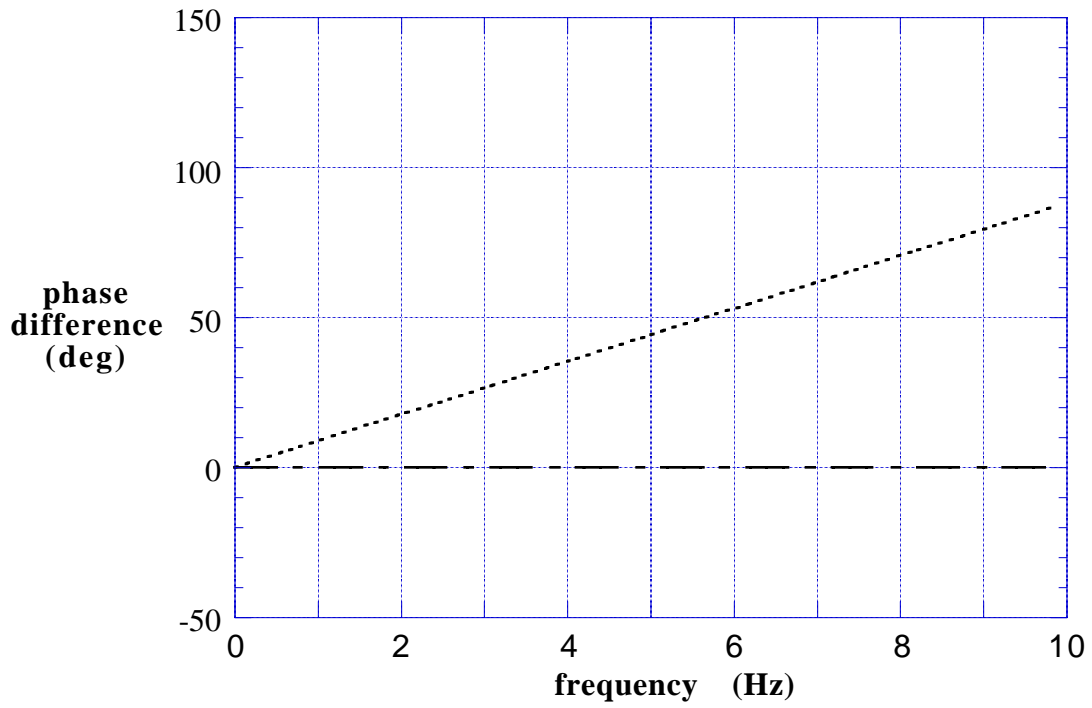
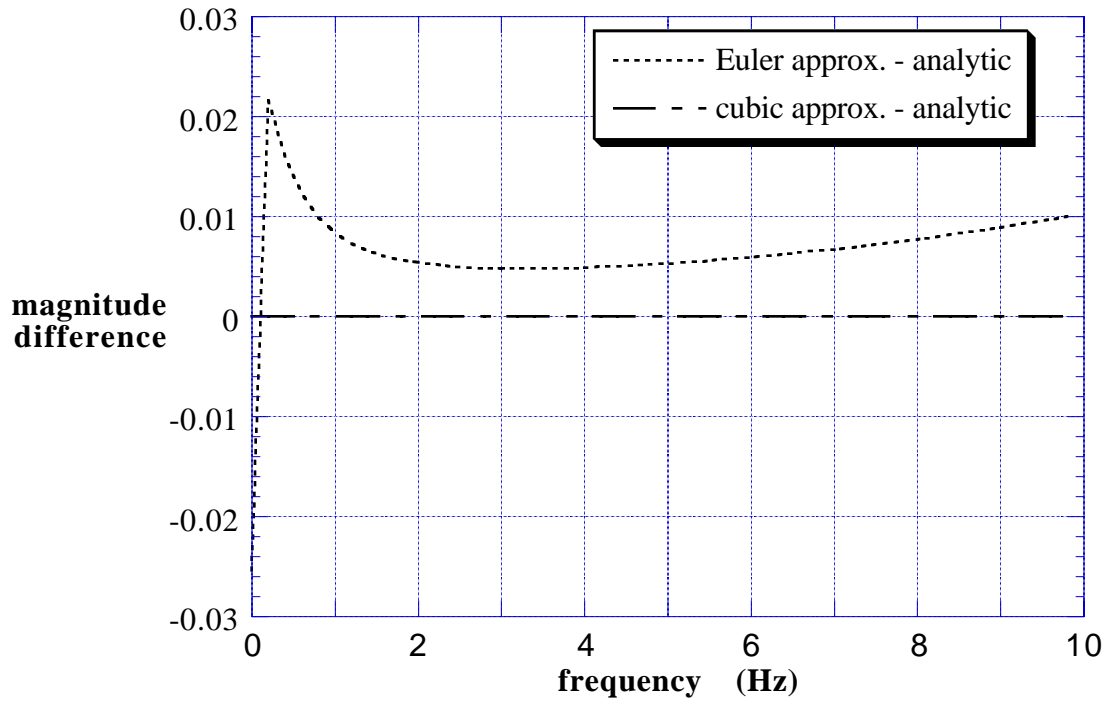


Figure 4 Differences for Finite Fourier Transform Calculations

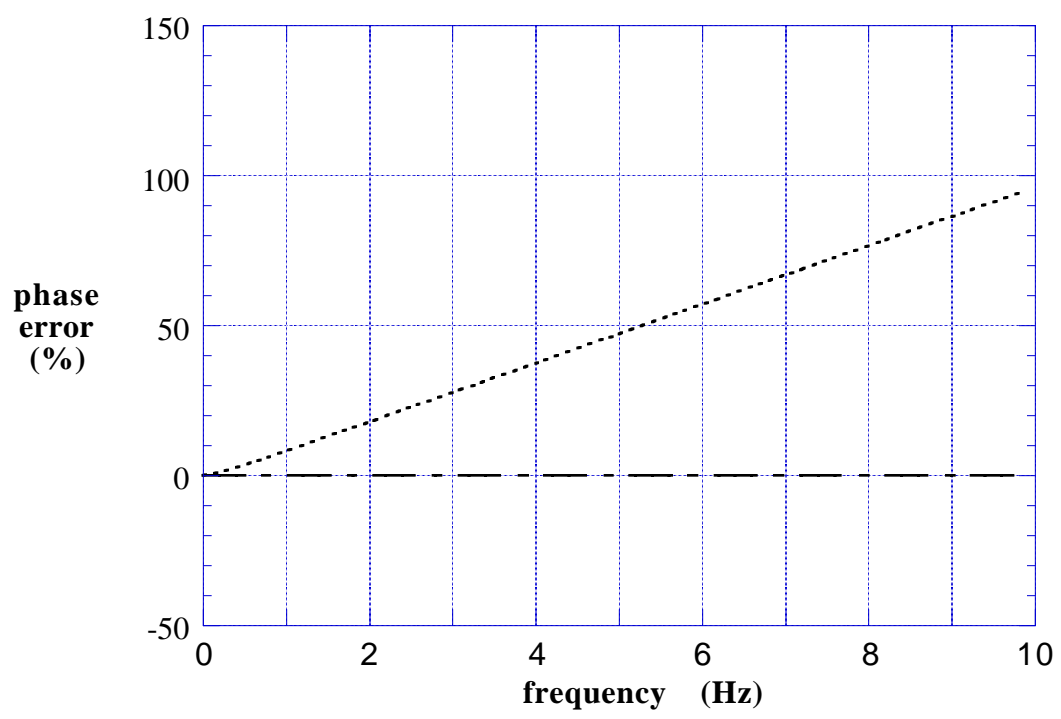
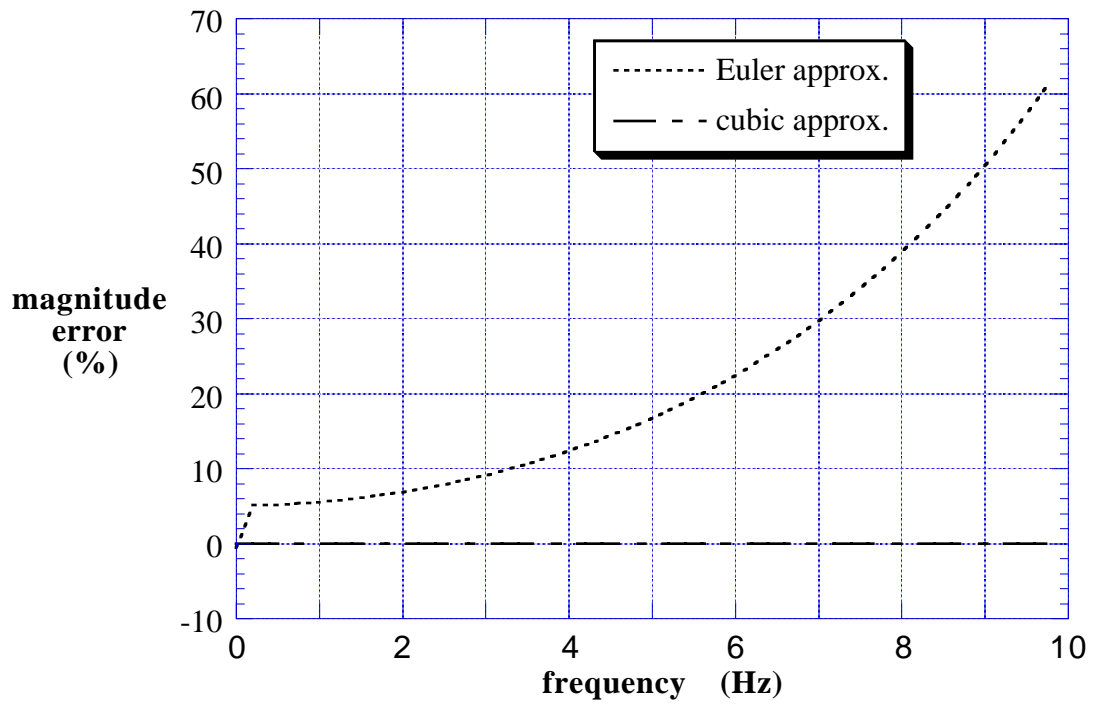


Figure 5 Percent Errors for Finite Fourier Transform Calculations

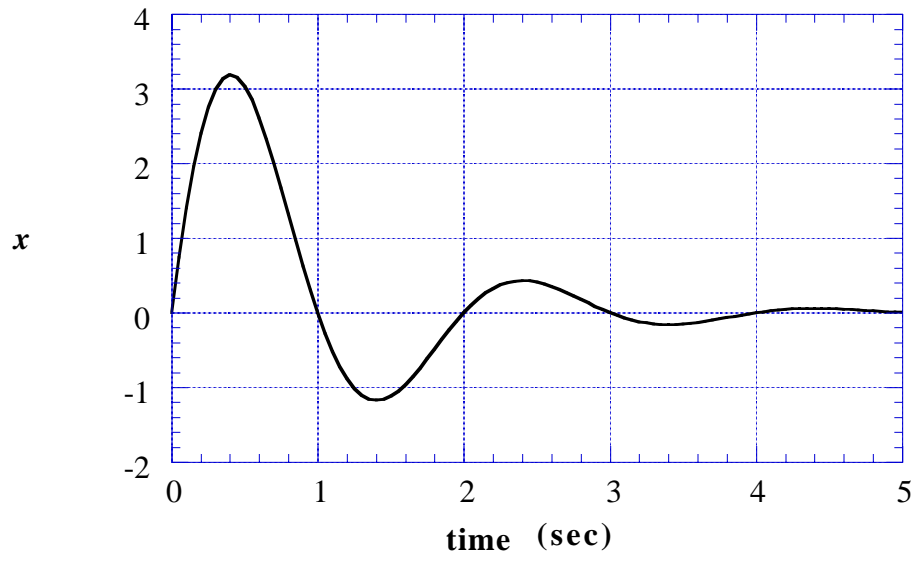


Figure 6 Example Time History

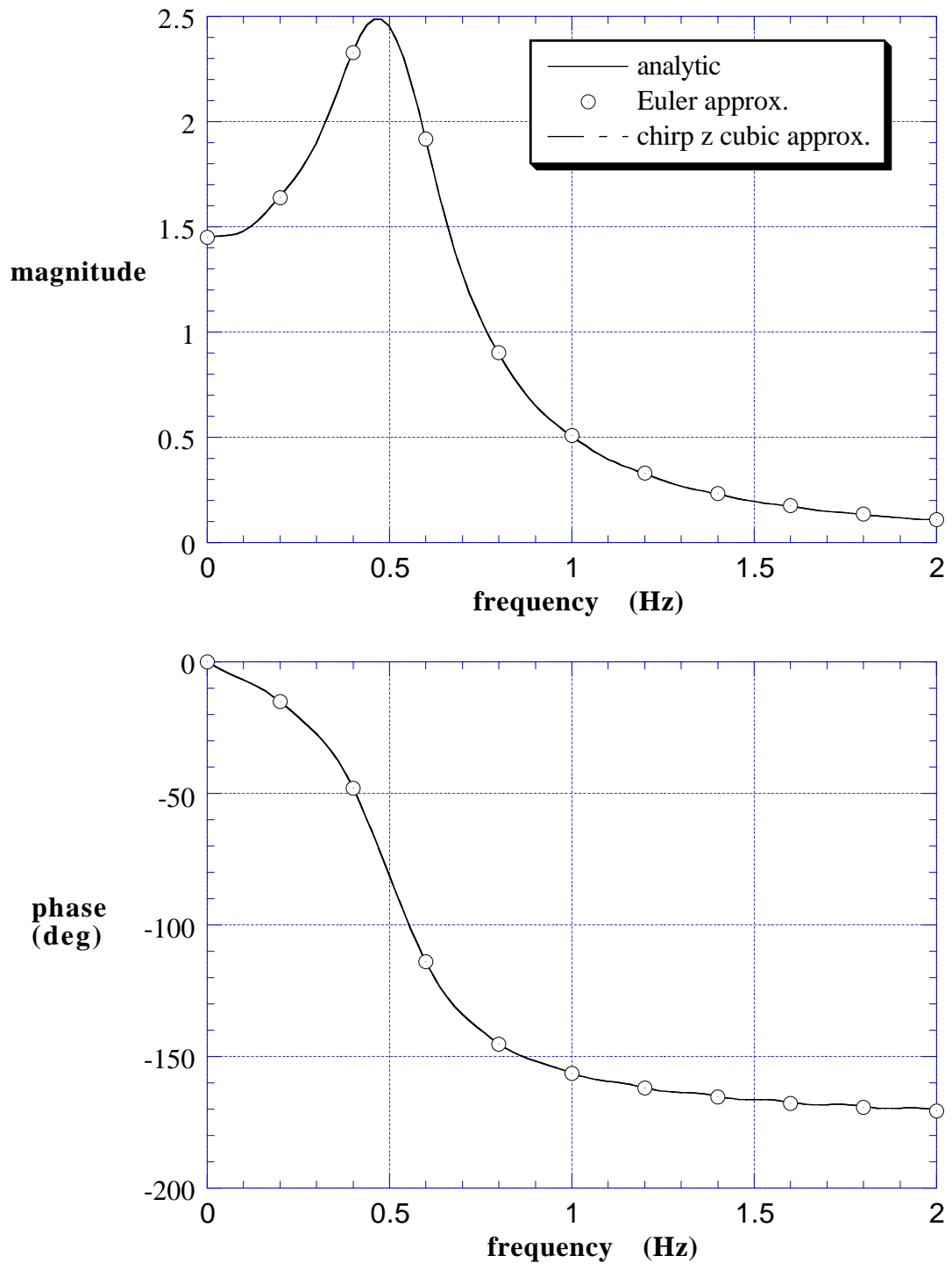


Figure 7 Finite Fourier Transform Calculation Comparison

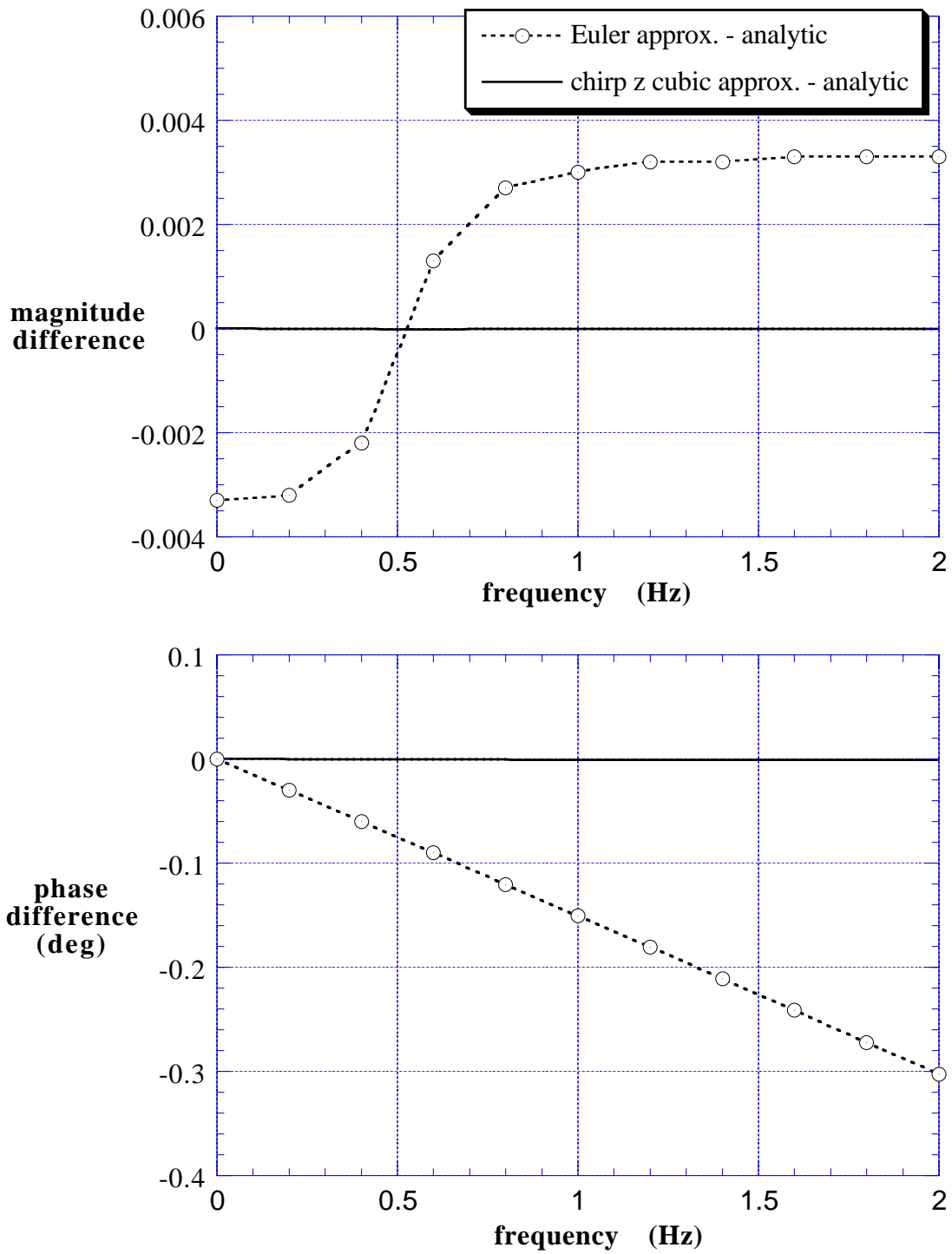


Figure 8 Differences for Finite Fourier Transform Calculations

**F-18 High Alpha Research Vehicle
Longitudinal Flight Test Maneuver 274b**

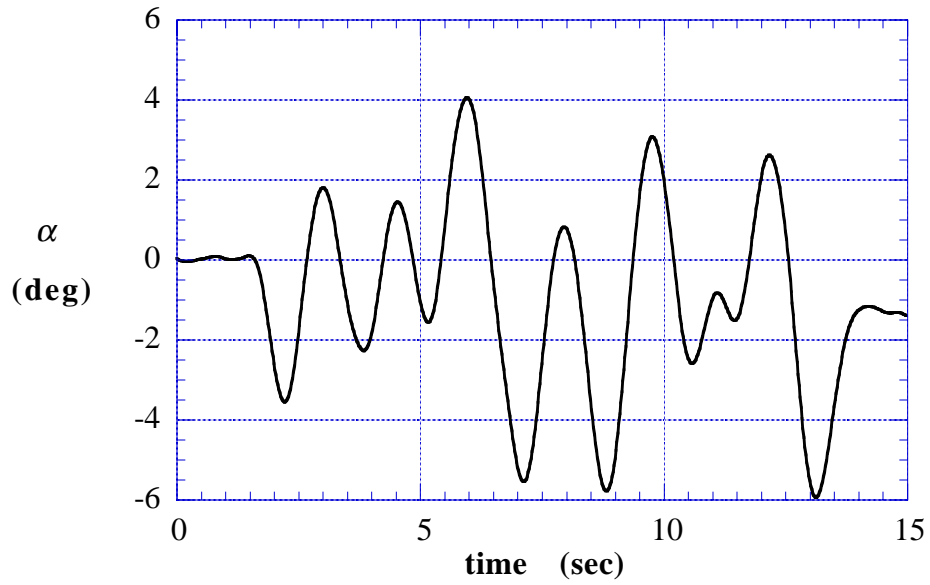


Figure 9 Angle of Attack Time History

**F-18 High Alpha Research Vehicle
Longitudinal Flight Test Maneuver 274b**

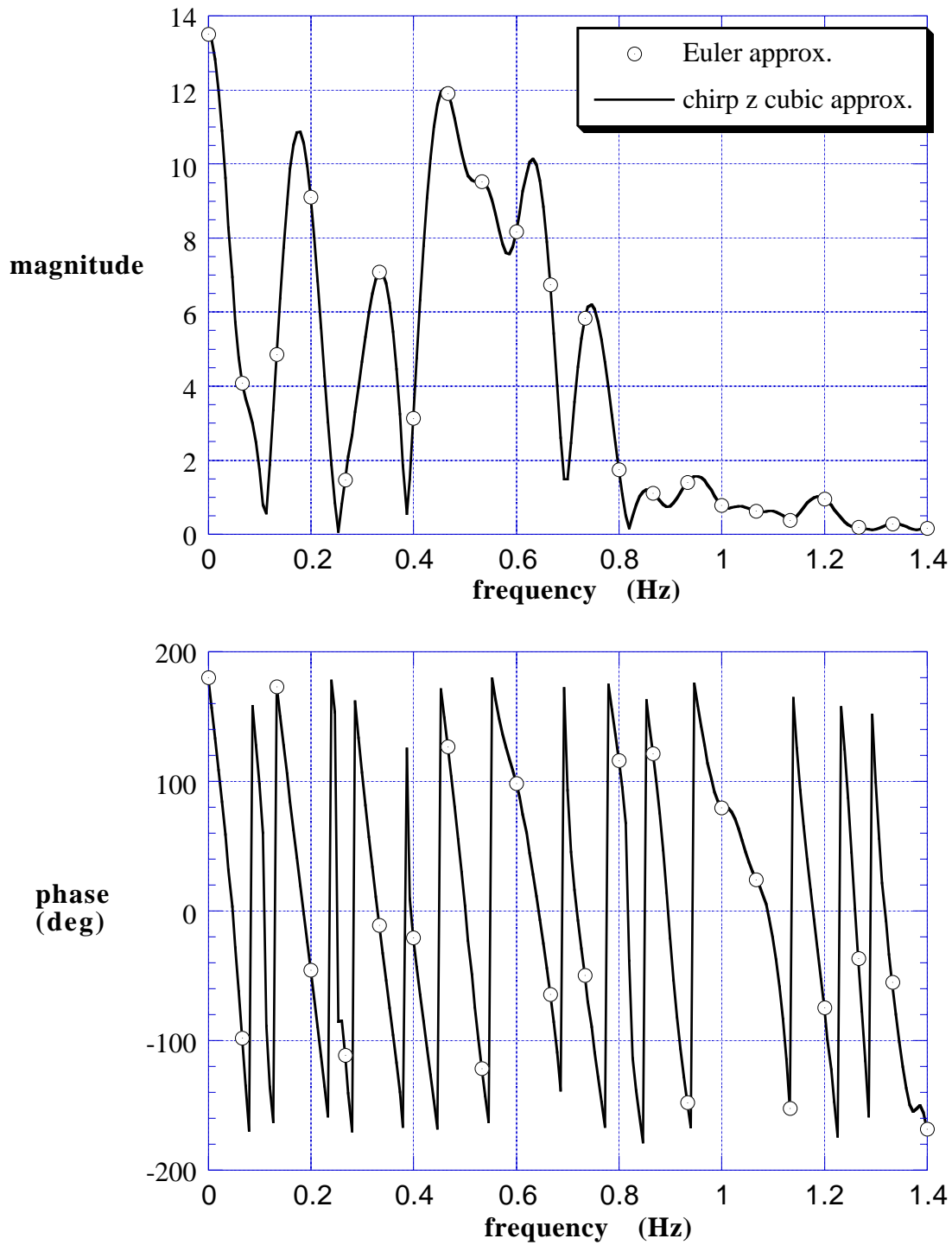


Figure 10 Finite Fourier Transform Calculation Comparison

**F-18 High Alpha Research Vehicle
Longitudinal Flight Test Maneuver 274b**

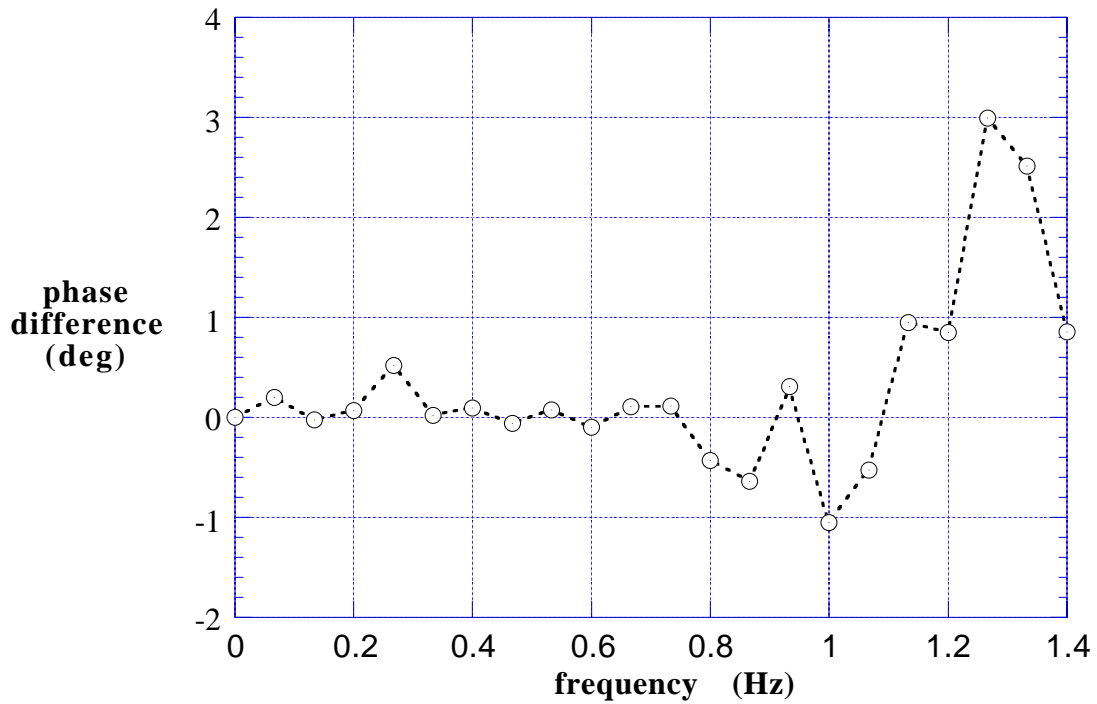
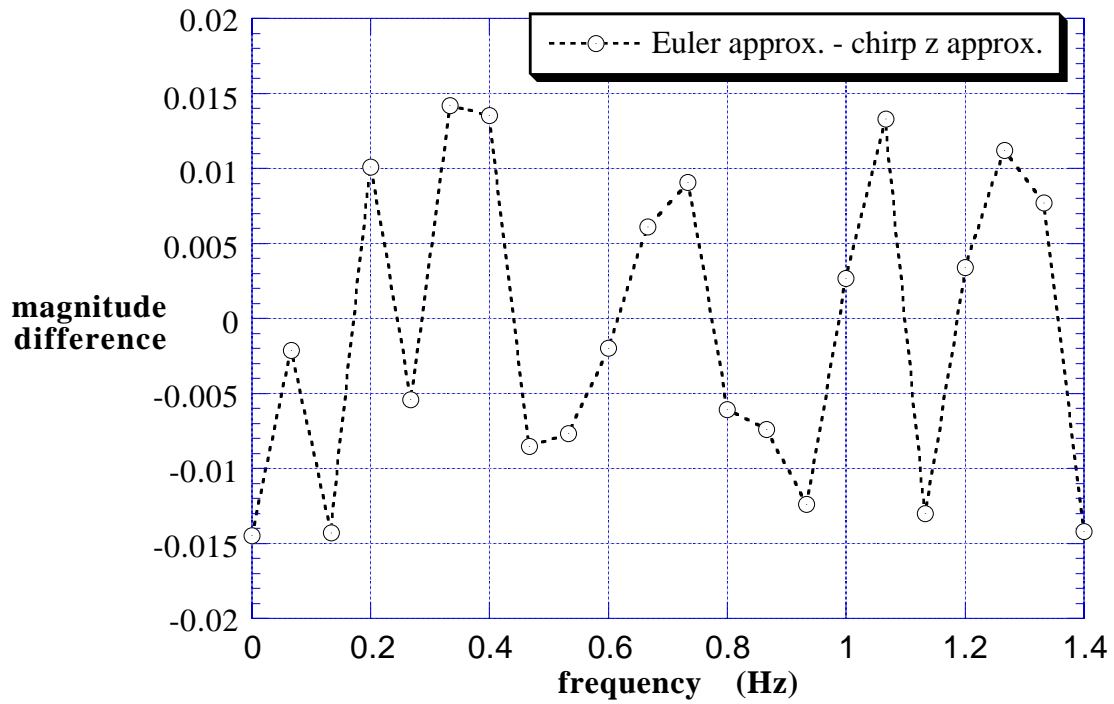


Figure 11 Differences for Finite Fourier Transform Calculations

**F-18 High Alpha Research Vehicle
Longitudinal Flight Test Maneuver 274b**

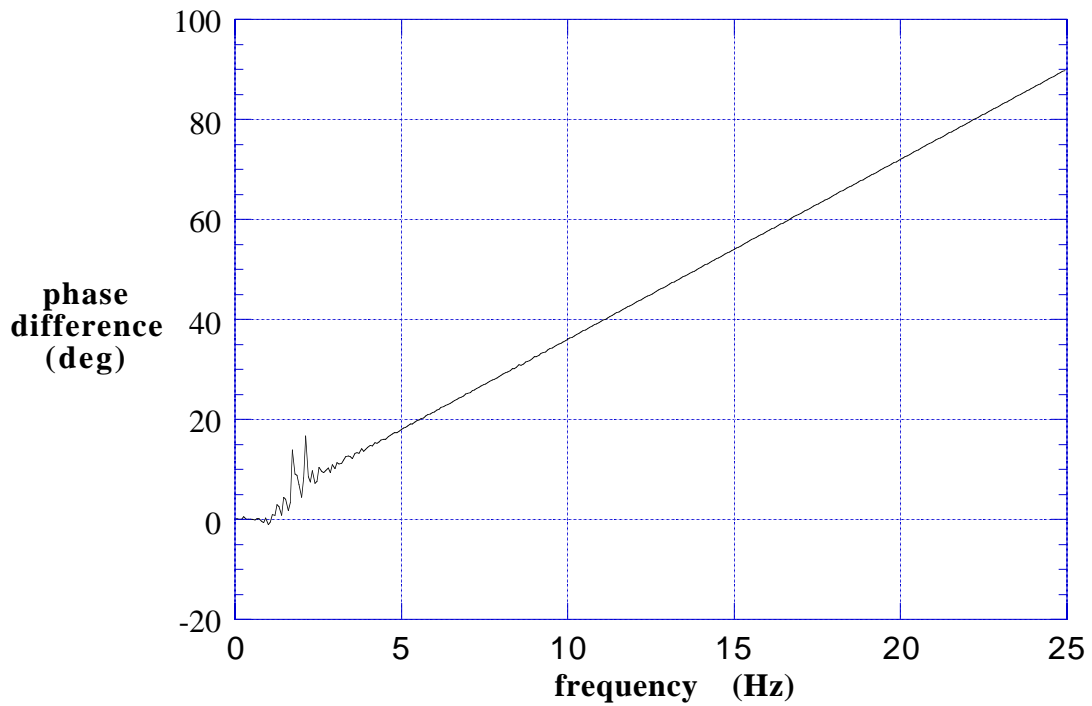
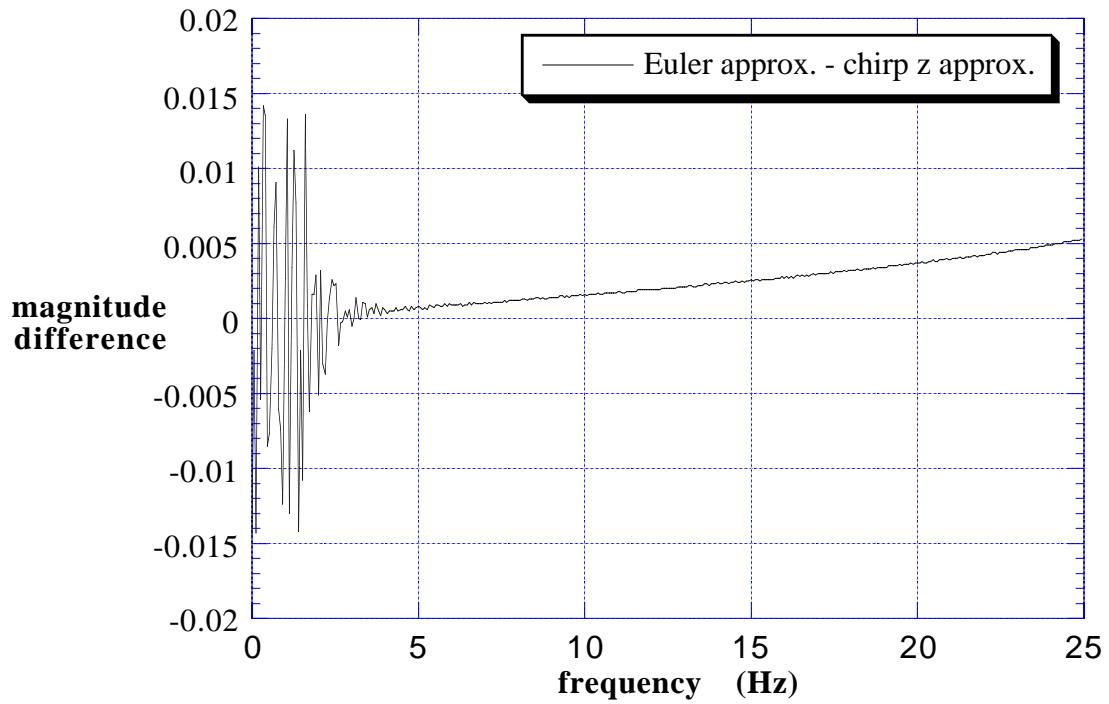


Figure 12 Differences for Finite Fourier Transform Calculations

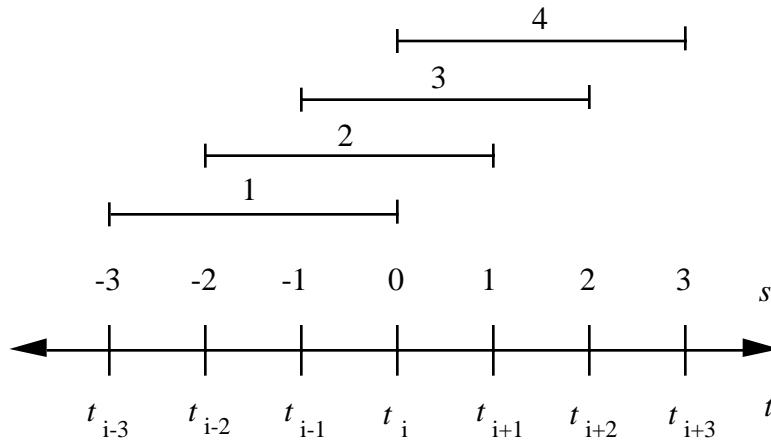


Figure A-1 Interior Interpolation

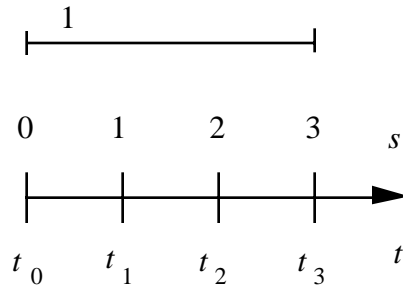


Figure A-2 First Interval Interpolation